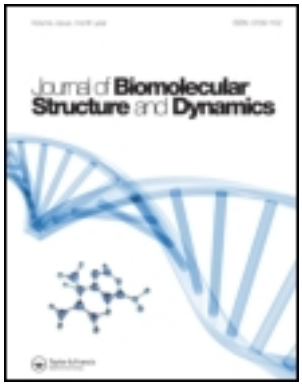

Journal of Biomolecular Structure and Dynamics
Publication details, including instructions for authors and subscription information:
http://www.tandfonline.com/loi/tbsd20

Molecular modeling study for conformational changes of Sirtuin 2 due to substrate and inhibitor binding

Sugunadevi Sakkiah [a], Meganathan Chandrasekaran [a], Yuno Lee [a], Songmi Kim [a] & Keun Woo Lee [a]

[a] Division of Applied Life Science (BK21 Program), Systems and Synthetic Agrobiotech Center (SSAAC), Plant Molecular Biology and Biotechnology Research Center (PMBBRC), Research Institute of Natural Science (RINS), Gyeongsang National University (GNU), 501 Jinju-daero, Gazha-dong, Jinju, 660-701, Republic of Korea

Version of record first published: 12 Jun 2012

To cite this article: Sugunadevi Sakkiah, Meganathan Chandrasekaran, Yuno Lee, Songmi Kim & Keun Woo Lee (2012): Molecular modeling study for conformational changes of Sirtuin 2 due to substrate and inhibitor binding, Journal of Biomolecular Structure and Dynamics, 30:3, 235-254

To link to this article: http://dx.doi.org/10.1080/07391102.2012.680026

Journal of Biomolecular Structure and Dynamics
Vol. 30, No. 3, 2012, 235–254

Molecular modeling study for conformational changes of Sirtuin 2 due to substrate and inhibitor binding

Sugunadevi Sakkiah, Meganathan Chandrasekaran, Yuno Lee, Songmi Kim and Keun Woo Lee*

Division of Applied Life Science (BK21 Program), Systems and Synthetic Agrobiotech Center (SSAAC), Plant Molecular Biology and Biotechnology Research Center (PMBBRC), Research Institute of Natural Science (RINS), Gyeongsang National University (GNU), 501 Jinju-daero, Gazha-dong, Jinju 660-701, Republic of Korea

Communicated by Ramaswamy H. Sarma

(*Received 26 November 2011; final version received 1 February 2012*)

Sirtuin is a member of NAD^+-dependent deacetylase family. The structural details of Sirtuin 2 (SIRT2) complex will be very useful to discover the drug which might have beneficial effects on various diseases like cancer, diabetes, etc. Unfortunately, SIRT2 complex structure is not available yet, hence molecular docking was carried out to dock the substrate (NAD^+ and acetylated lysine) and inhibitor (sirtinol) in the NAD^+ binding site. The suitable binding orientation of substrate and inhibitor in the SIRT2 active site was selected and subjected to 5 ns molecular dynamics simulations to adjust the binding orientation of inhibitor and substrate as well as to identify the conformational changes in the active site. The result provides an insight about 3D SIRT2 structural details as well as the importance of F96 in deacetylation function. In addition, our simulations revealed the displacement of F96 upon substrate and inhibitor binding, inducing an extended conformation of loop3 and changing its interactions with the rest of SIRT2. We believe that our study could be helpful to gain a structural insight of SIRT2 and to design the receptor-based inhibitors.

Keywords: sirtuin; molecular dynamics simulation; molecular docking; electrostatic potential; GROMACS; LigandFit; sirtinol

Introduction

Histone acetyltransferases proteins acetylate the ε-N-acetyl lysine in histones and this process is reversed by histone deacetylases (HDACs) (Mai et al., 2005) family of proteins. In humans, HDACs have been categorized into four different classes (I–IV), which depends on its sequence homology and phylogenetic analysis (Sakkiah et al., xxxx). Class-I contains HDACs 1–3 and 8, Class-II comprises of 4–7 and 9–10 HDACs, Class-III HDAC, silent information regulator2 (Sir2 or sirtuin), not showing any sequence similarity to other class of HDACs, and HDAC 11 comes under the Class-IV (Witt, Deubzer, Milde, & Oehme, 2009). The Class-I, -II, and -IV are similar to each other in their catalytic cores as well as it utilizes the zinc (Zn) ion to deacetylate the histone and nonhistone proteins, but in the case of Class-III instead of Zn ion NAD^+ is required for its function (Metoyer & Pruitt, 2008). Here, we mainly focused on a unique ancient family of NAD^+-dependent deacetylase HDAC (sirtuin) (Imai et al., 2000; Landry et al., 2000), which cleaves the acetyl group from acetylated proteins such as histones and also from several transcription factors (Huhtiniemi et al., 2006). Sirtuins are required for transcriptional silencing, regulation of apoptosis, fat mobilization, DNA recombination and repair, axonal protection and lifespan regulation (Sakkiah et al., 2009). In several organisms, sirtuins are unique among many groups of proteins related to aging, metabolism, and stress tolerance. At present, in mammals seven homologs of sirtuins have been reported and named as SIRT1–7 (Guarente, 2007; Haigis & Guarente, 2006), which are all closely related with health and lifespan. Sirtuin enzymes contain a conserved NAD^+-dependent catalytic core domain which can act as either a mono-ADP-ribosyltransferase (ART) or a NAD^+-dependent deacetylase (DAC) or both, but shows a variation in the N-and/or C-terminal (Sakkiah et al., 2009).

Sirtuin apparently mediates the life-extending effects in different organisms by targeting various pathways. SIRT1, present in nucleus and modulates as cytosolic targets, is a NAD^+-dependent deacetylase which alters the several physiological functions including control of gene

*Corresponding author. Email: kwlee@gnu.ac.kr

ISSN 0739-1102 print/ISSN 1538-0254 online

http://dx.doi.org/10.1080/07391102.2012.680026
http://www.tandfonline.com

expression, metabolism, and aging (Longo & Kennedy, 2006). SIRT1 deacetylase many key transcription factors and cofactors such as p53 (Vaziri et al., 2001), forkhead protein (Brunet et al., 2004; Motta et al., 2004), peroxisome proliferation activating receptor gamma coactivator-1γ (Rodgers et al., 2005), and nuclear factor-κB (Yeung et al., 2004) by affecting the crucial cellular pathways involved in stress resistance and metabolism. Another homology, SIRT2 is predominantly present in cytoplasmic and mainly deacetylase tubulin (Dryden et al., 2003). During G2/M transition and mitosis, SIRT2 is localized in nucleus and deacetylates histone H4 that leads to the formation of condensed chromatin (Baker, Sept, Joseph, Holst, & McCammon, 2001). SIRT2 involves in major pathways like IGFs/gluconeogenesis, cardiomyopathy, cell cycle regulation, and apoptosis which leads to diabetes/obesity, cardiovascular, cancer, and neurodegenerative diseases, respectively. It has been identified as an ideal molecular target in the drug discovery process for the treatment of a series of diseases like cancer, Alzheimer's, Parkinson's, etc. Recent studies also suggest that the potential roles of SIRT2 in development of neurodegenerative diseases (Huhtiniemi et al., 2008) and inhibition of SIRT2 rescue α-synuclein toxicity in a cellular model of Parkinson's disease (Hiratsuka et al., 2003; Outeiro et al., 2007). SIRT3, 4, and 5 are mainly mitochondrial proteins and SIRT6 and 7 are present in the nucleus and nucleolus, respectively (Michishita, Park, Burneskis, Barrett, & Horikawa, 2005; Vaquero et al., 2006). There is a structural conservation among the sirtuin families that contains a conserved enzymatic core comprising the Rossmann fold domain and small domain that is composed of Zn-binding and helical domains (Sakkiah et al., 2009). Biochemical studies of sirtuin activity show that deacetylation occurs stoichiometrically with hydrolysis of glycosidic bond between nicotinamide and ribose of NAD^+ to form a covalently bound *O*-alkylamidate intermediate (Westphal, Dipp, & Guarente, 2007). Two different structure-based mechanisms for nicotinamide cleavage reaction of sirtuin have been proposed by Avalos et al. (2002). Zhao et al. (2004) mentioned that NAD^+ binds in the two different conformations in sirtuin pocket such as "productive" and "nonproductive" forms. In productive conformation, NAD^+ buries the positive charge of nicotinamide ring in a conserved pocket known as the C-site consist of highly hydrophobic residues that disrupts the resonance of delocalized electrons of nicotinamide ring through carboxamide moiety distortion. In nonproductive conformation, the nicotinamide ring fails to burry in the C-site (Avalos, Boeke, & Wolberger, 2004).

Sirtuin2 structure details

Totally 389 residues are present in SIRT2, out of these 323 amino acids are crystallized at 1.7 Å resolution, which provided a strong base to understand the structural behavior of SIRT2 (Finnin, Donigian, & Pavletich, 2001). The catalytic core has an elongated shape with two domains such as large and small domains. The large domain contains the Rossmann fold, comprised of six parallel β-sheets surrounded by six α-helices. The small domain was classified into Zn-binding and helical domains (Satoh et al., 2010) (Figure 1(a)). The Zn-binding domain consists of three anti-parallel β-sheets, 1

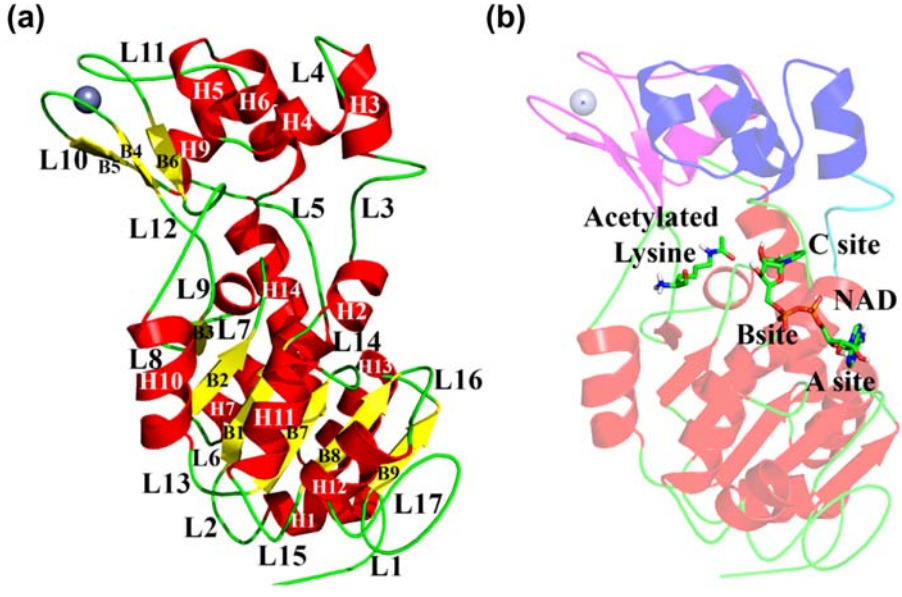

Figure 1. (a) Structural details of SIRT2. (b) Helical domain (blue), zinc binding domain (magenta), zinc (gray), large domain (red), L3 (cyan), NAD^+, and acetylated peptide are represented in stick (green).

α-helix, and Zn was anchored by four cysteine residues (C195, C200, C221, and C224) conserved across all classes of Sir2-like enzymes and the helical domain comprised of four helices (two short and two long helices). The large and small domains are connected by four crossovers (C) of polypeptide chain, C1: G92-Y104; C2: P139-Y145; C3:A186-T192; and C4: D231-P240. The NAD^+ and acetylated proteins are binds in the large grove formed between the small and large domain (Figure 1(b)). The NAD^+ binding pocket was classified into three sites: A, B, and C. A-site contains G86, A87, N97, G261, N286, E288, G323, C324, and K343 among these N286 and E288 forms a hydrogen bond with adenine ribose 2′ and 3′ OH groups, N97 and A85 poised to interact with phosphate oxygens, and the remaining residues surround the adenine base of NAD^+. Only two residues are present in B-site, H187 and Q167, forms the hydrogen bond with 3′OH of nicotinamide ribose and also plays an important role in sirtuin mechanism (Finnin et al., 2001). The C-site involved in hydrolysis and polarization of NAD^+ glycosidic bond which contains highly conserved residues like S88, H149, N168, I169, and D170. There are four conserved loops connecting the small and large domains such as loop3 (L3), loop9 (L9), loop11 (L11), and loop15 (L15) (Figure 1(a)).

Still now, there is a lack of data which provides the binding orientation of acetylated lysine and NAD^+ (substrates) and sirtinol (inhibitor) in SIRT2 active site. The Apo-form of SIRT2 fails to insight the dynamic or conformational changes due to the binding of substrate and inhibitor. Understanding the dynamic behavior of protein would be vital to interpret its binding mechanism as well as to design small molecules to inhibit its functions. Hence, the research on aspects of substrate and inhibitor binding orientations are far from complete and more research is required. In this study, we present the first attempts to use molecular docking to form a complex SIRT2 and molecular dynamics (MD) simulation to gain insights into the dynamic properties of wild type (WT) and mutants (F96A and F96Y) SIRT2. MD simulation is an alternative and effective technique to gather additional information regarding the small molecule/or protein that induced conformational changes in proteins. Totally, nine independent MD simulations were carried out to explore dynamic behavior and proper binding orientations of substrate and inhibitor. Our results strongly suggested that L3 conformational rearrangements and F96 could be responsible in triggering or stimulating the SIRT2 activity.

Methods and materials

Protein and small molecules preparation for molecular docking

To date, only one SIRT2 Apo-form is available in the protein data bank (PDB) (Berman et al., 2000) and there is no human sirtuin2 complex structure. Molecular docking studies were preformed to insight the structural details due to the presence of substrates and inhibitor. Information on the interaction properties of substrate/inhibitors are required to efficiently design new inhibitors. Hence to produce a complex SIRT2, Apo-form of SIRT2 (PDB: 1J8F, resolution 1.70 Å) was used as a receptor and the hanging N-terminal helix (G34-F45) was removed. *LigandFit* (Venkatachalam, Jiang, Oldfield, Waldan, & LigandFit, 2003) from Discovery Studio v2.5 (DS, http://www.accelrys.com) was utilized to dock the substrates and inhibitor in SIRT2 active site. Before initiating the docking study, the receptor was neutralized by removing the water molecules and hydrogen atoms were added by applying CHARMm force field (Brooks et al., 1983). The added hydrogen atoms attained its suitable orientations in receptor by applying position restrained energy minimization. The 2D format of NAD^+, acetylated lysine, and inhibitor were drawn using ChemSketch and converted into 3D format by exporting into DS. To obtain the most stable energy-minimized conformation of these molecules, maximum number of 255 conformations were generated for each by applying Poling algorithm (Smellie, Teig, & Towbin, 1995) using the *Best Conformation* module.

Molecular docking strategy

LigandFit module was classified into three stages: (i) docking, attempt is made to dock a ligand into a user defined binding site, (ii) in-situ ligand minimization, and (iii) scoring: various scoring functions were calculated for each pose of the ligands. The protein was prepared by removing the solvent molecules and hydrogen atoms before adding atom types with the CHARMm force field (Brooks et al., 1983). After the protein preparation, the suitable binding site for substrates and inhibitor was identified before initiating the docking process. The active site of protein was represented as a binding site and identified using two methods: firstly, based on the shape of receptor using "eraser" algorithm and secondly, volume occupied by the known ligand poses already in an active site. In our case, the first method, eraser algorithm was applied to detect the suitable binding pocket for substrates and inhibitor. The observed binding site of SIRT2 was verified by comparing the volume occupied by NAD^+ in yeast sirtuin-complex (PDB ID: 1SZC). And also, the active site residues of NAD^+ binding pocket of SIRT2 were confirmed by multiple sequence analysis of the sirtuin family and based on the literature (Avalos, Bever, & Wolberger, 2005; Zhao et al., 2004). To confirm the binding orientation of inhibitor in SIRT2, sir2Af2 sirtuin (PDB ID: 1YC2) (Avalos et al., 2005) was used as a reference complex structure to compare with the docked SIRT2–inhibitor complex. The docking process saved top 25 conformations for each molecule

Table 1. Summary of nine model systems for molecular dynamics simulations.

No.	Acronyms	System details	Structure	Protein atoms	Water molecules	Na^+ ions
1	WT_Apo	WT Apo form	SIRT2	3038	20,486	4
2	WT_Sub	WT substrate complex	SIRT2 + NAD^+ + acetylated lysine	3110	20,454	1
3	WT_Inhi	WT inhibitor complex	SIRT2 + sirtinol	3071	20,461	4
4	F96A_Apo	F96A Apo form	F96A SIRT2	3027	20,499	4
5	F96A_Sub	F96A substrate complex	F96A SIRT2 + NAD^+ + acetylated lysine	3101	20,440	1
6	F96A_Inhi	F96A inhibitor complex	F96A SIRT2 + sirtinol	3060	20,468	4
7	F96Y_Apo	F96Y Apo form	F96Y SIRT2	3039	20,488	4
8	F96Y_Sub	F96Y substrate complex	F96Y SIRT2 + NAD^+ + acetylated lysine	3113	20,433	1
9	F96Y_Inhi	F96Y inhibitor complex	F96Y SIRT2 + sirtinol	3072	20,461	4

based on dock score after the energy minimization using the smart minimizer method, which begins with the steepest descent algorithm and followed by the conjugate gradient method.

Molecular dynamics simulation

The best SIRT2-complexes from the docking result have been subjected to MD simulations to refine the reasonable binding mode of substrates and inhibitor. Totally, nine independent systems were prepared for MD simulations which are summarized in Table 1.

The MD simulation performed to gain an insight into processes on an atomistic scale. It has a unique ability to directly describe the dynamic properties of protein structure-based on time-dependent positions of all atoms in the systems. In our study, the classical MD simulations were performed using GROMACS 3.3.0 software package (GROMACS, 2002; McGovern, Fau-Shoichet, & Shoichet, 2003; Van Der Spoel et al., 2005) by applying leap-frog integration steps to solve the equations of motion. Apo-form, SIRT2 in presence of substrates, and inhibitor for wild type (WT) and mutants (F96A and F96Y) systems are prepared for MD simulations. GROMOS96 (Berendsen, van der Spoel, & van Drunen, 1995; Lindahl, Hess, & van der Spoel, 2001) force field, describes the inter-atomic interactions, has been applied to permit the flexible interactions and to observe ligand sustainability in binding pockets. The molecular topology file for substrates and inhibitor was constructed by submitting into PRODRG web server (Schuttelkopf & Aalten, 2004). No new atom types are included for substrates and inhibitor, the atom charges and force constants are defined in GROMOS96 force field. The nine systems were solvated by generating a cubic box with 1 nm as minimum distance between the protein and the edge of the box. The SP3 (Berendsen, Postma, van Gunsteren, & Hermans, 1981) water model was used to create an aqueous environment and the periodic boundary condition was applied in all directions. The systems were neutralized by adding Na^+ ions by replacing the water molecules. This was done by random substitution of water molecules with ions at the most favorable electrostatic potential positions. A cut-off distance was set for short-range interactions: 0.9 nm for van der Waals interactions and 1.4 nm for electrostatic interactions. LINCS (Hess, Bekker, Berendsen, & Fraaije, 1997) and SETTLE (Miyamoto & Kollman, 1992) algorithm was used to constrain the bond length and geometry of water molecules, respectively. Energy minimization was employed to relieve the unfavorable contacts present in each system by using steepest decent algorithm with a tolerance of 2000 kJ mol^{-1} nm^{-1} and subjected to 50 ps equilibration run. Subsequently, to relax the solvent molecules present in systems, 100 ps of position restrained runs were performed (Sakkiah, Thangapandian, John, & Lee, 2011). These equilibrated systems were subjected to 5 ns production MD simulation with a timestep of 2 fs at constant temperature (300 K), pressure, (1 atm) and number of particles, without any position restraints (Berendsen, Postma, van Gunsteren, DiNola, & Haak, 1984). The representative structures were selected and analyzed using the standard GROMACS package tools.

Electrostatic potential surface calculation

Electrostatic potential surface was calculated using the electrostatic potential module/DS for WT and mutants Apo-form, presence of substrates and inhibitor representative structures obtained from the last 2 ns of MD simulations. The electrostatic potential module runs the Delphi program that uses a two-dielectric implicit method and a finite difference method to solve the Poisson–Boltzmann equation to calculate the spatial distribution of the electrostatic potential and potential of protein atoms. The default parameters were used in the calculations.

Result and discussion

Molecular docking

Since the absence (Grozinger, Chao, Blackwell, Moazed, & Schreiber, 2001) of structural details of complex SIRT2, molecular docking was carried out. Molecular docking approach is one of the reputable methods to find the solution for many difficult

problems such as disclosing the ligand orientations in protein active sites. *LigandFit* was used to gain an insight into the most probable binding conformation of small molecules in protein active sites. Docking accuracy was measured by the relative true binding mode of small molecules in receptor active sites, which determined the quality of docking methodology. The SIRT2 Apo-form was selected as a receptor from PDB to make visible binding orientation of substrates and inhibitor in active sites. The docked SIRT2 with substrates and inhibitor are well placed (occupied) in the suitable binding pocket and showed all necessary interactions which are reported in literature (Avalos et al., 2005; Zhao et al., 2004). SIRT2-substrate complex, NAD^+ forms an hydrogen bond interactions with NAD^+ binding sites: A-site, A85: HN with O1A and O4B, G86: HN with N3A and O4B, and N286:HD22 with N3A, in B-site both the residues such as Q167: HE22 with O3D and H131HE2 with O3D, and only two residues from C-site shows an hydrogen bond with NAD^+, I169: HN and D170: HN had shown an hydrogen bond with O7Nl. The acetylated lysine in the SIRT2-substrate complex binds in the conserved hydrophobic pocket nearby NAD^+ binding. SIRT2–inhibitor, the inhibitors forms hydrogen bond interactions with the Q167, I169, and D170 (Sakkiah et al., xxxx) which are the important residues present in C-site. Finally, sirtuin complexes were confirmed by the critical interactions between substrates/inhibitor and amino acids in SIRT2 active site. SIRT2–substrates and SIRT2–inhibitor complexes, which shows the good interactions with the critical residues in the active site, were overlaid with yeast and *Af2* sirtuin complexes to cross-check the binding orientations of substrates and inhibitor. The overlay of the SIRT2-complexes with substrates and inhibitors shows similar orientation as reported in yeast and *Af2*. Hence, the best SIRT2-complexes were subjected to MD simulation to observe its structural changes due to the presence of substrates and inhibitor.

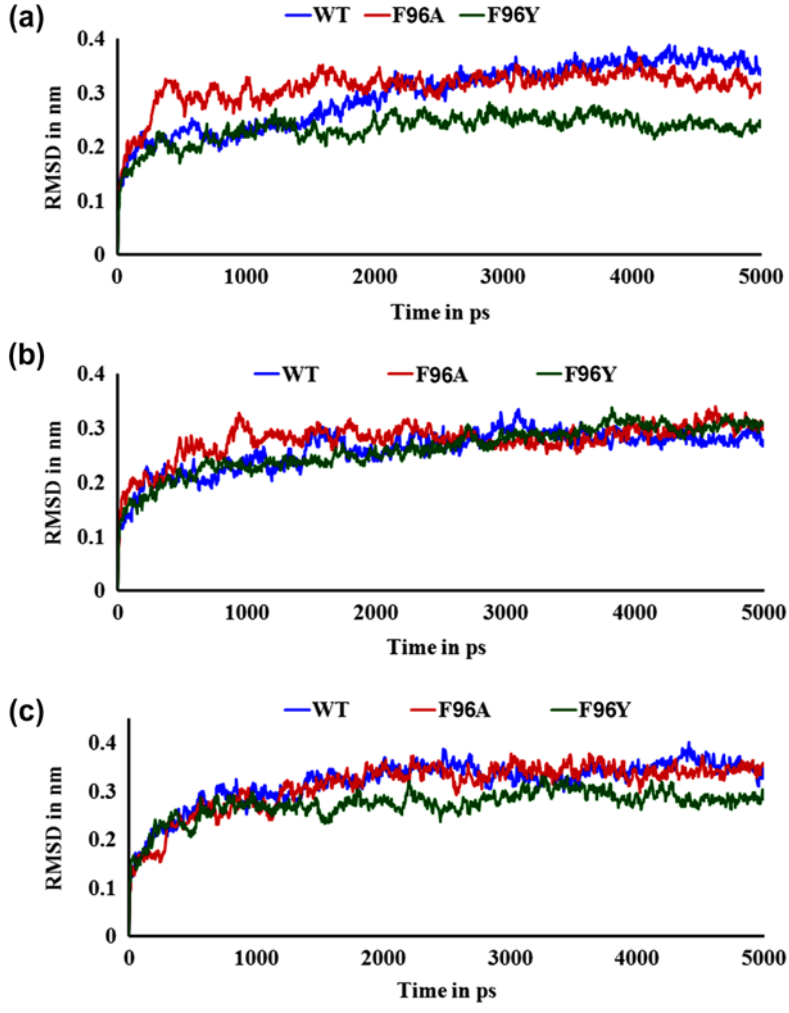

Figure 2. Root mean square deviation (RMSD) profiles of Cα atoms. (a) Apo-form, (b) SIRT2 bound with substrate, and (c) SIRT2 with inhibitor. Independent fittings are used in each RMSD profile with respect to the initial structure.

Molecular dynamics simulation

X-ray crystal structure acts as a starting point for exploring the relationship between structure and function, but generally it fails to describe the dynamic properties of protein. To overcome this, we utilized MD simulation to disclose the atomistic insight, positioning of backbone, and side-chain atoms due to substrate and inhibitor binding. MD simulation was employed to analyze the structural behavior of SIRT2 Apo-form as well as in presence of substrates and inhibitor over a specific time span of 5 ns for WT, F96A, and F96Y. Herein, the simulation results revealed the changes in secondary structure and the importance of C-site of NAD^+ binding pocket in presence of NAD^+ and inhibitor. The following results are based on nine MD simulation systems of SIRT2 (Table 1) including Apo and complexes of WT, F96A, and F96Y. The stability and fluctuation of proteins during the simulations were confirmed by root mean square deviation (RMSD) and root mean square fluctuation (RMSF) of the protein Cα-analysis, respectively.

Stability of SIRT2 structures during molecular dynamics simulation

MD simulations were carried out for WT and mutants: Apo-form, bound with substrates, and inhibitor. The structure stability of nine systems was confirmed by plotting RMSD of Cα-atom. To find, the regions which exhibit the significant residue fluctuation throughout MD simulation were analyzed by the progression of RMSD and RMSF of protein Cα atoms. The two dimensional RMSD plot for each system was obtained throughout the trajectory by keeping the starting structure ($t = 0$) as a function of time (Figure 2). The RMSD plot confirmed that all WT systems were stabilized in the last 2 ns,

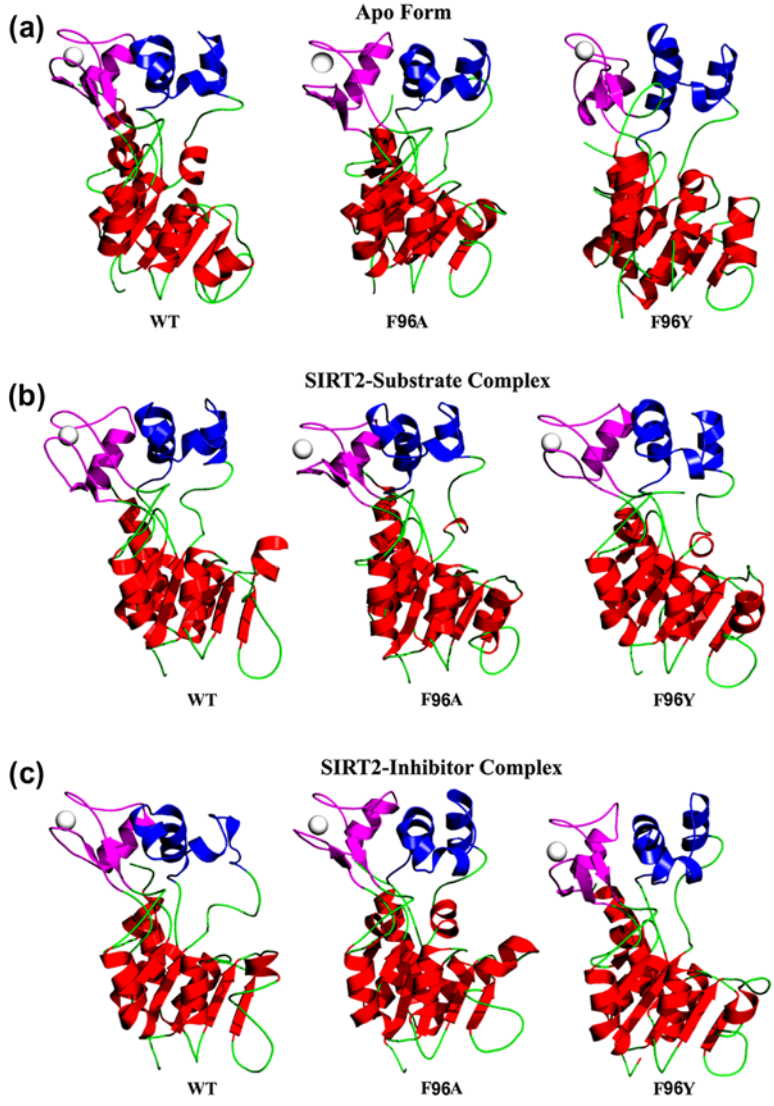

Figure 3. The representative structure of SIRT2 from nine systems, the large domain (red), helical domain (blue), and zinc binding domain (magenta). Substrate and inhibitor are not shown here for its clear view.

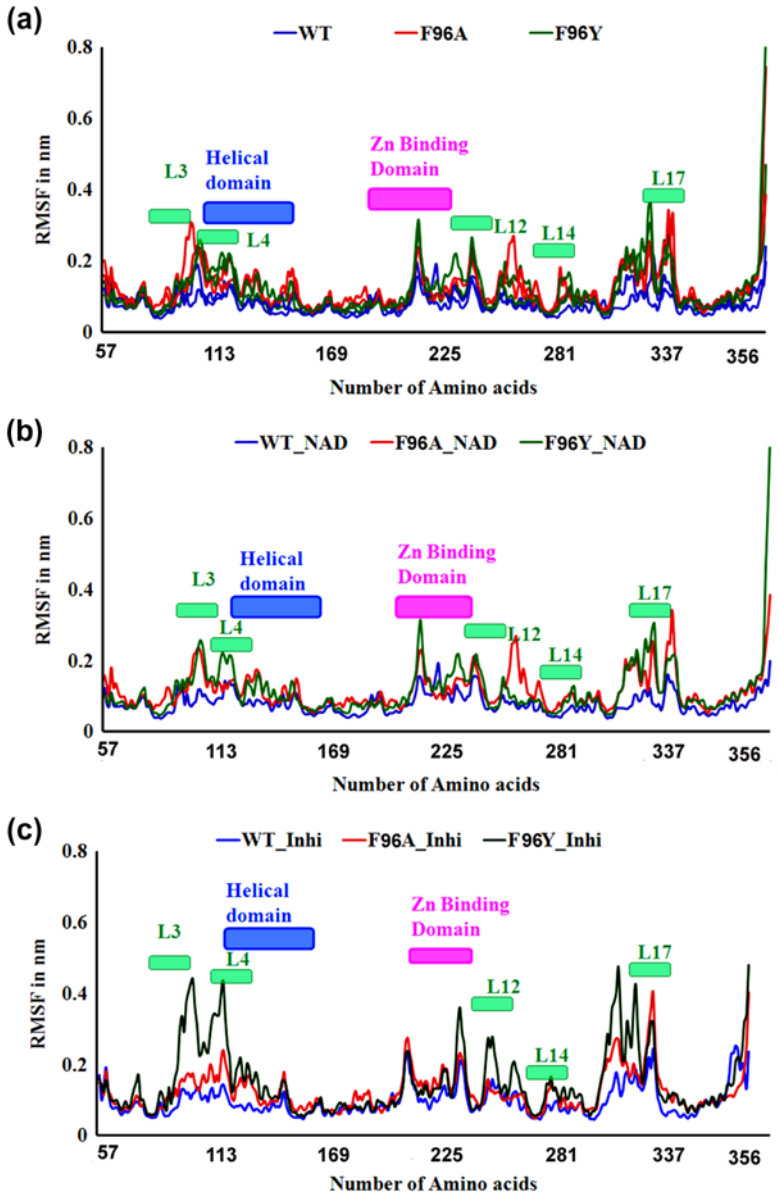

Figure 4. Local conformational changes indicated by atom-positional root mean square fluctuations (RMSF) calculated with respect to the average structure (a) Apo-form, (b) bound with substrate, and (c) bound with inhibitor.

WT_Apo and WT_Inhi had shown deviation between 0.33 and 0.35 nm, but the WT_Sub shows the value between 0.26 and 0.28 nm. We observed that WT_Apo and WT_Inhi showed more deviation (>0.3 nm) compared with the WT_Sub. The above analysis assured that the substrate binding will play a major role in protein stability throughout the simulation. Comparing the WT_Apo and WT_Inhi with mutants, in both cases F96Y was stabilized between 0.25 nm and 0.30 nm, but F96A shows the value greater than 0.30 nm to become stable. Interestingly, in the presence of substrate the WT and mutants systems were stabilized in the same range (∼0.3 nm). The last 2 ns RMSD plot of each system showed the stable RMSD values confirmed the protein stability. Hence, the representative structure (closest RMSD frame to the average structure) from the last 2 ns was selected for further structural comparison is depicted in Figure 3.

Flexibility of the residues

The relative flexibility of each system was characterized by plotting RMSF to the representative structure for both WT and mutants. RMSF of MD simulation trajectories has examined to explain the deviation of RMSD in Apo-form, complexes in WT and mutants. RMSF analyzes aid to estimate the flexibility of each residue along the

polypeptide chain, Cα atom of a particular residue averaged over the entire simulation time (Rodgers et al., 2005). It was significant to plot RMSF of Cα atoms (analogous to crystallographic B-factors) to find the more flexible regions of protein throughout the simulation. Results showed that all systems followed a similar pattern of fluctuation during 5 ns of simulation. The α-helices and β-strands have shown considerable deviation and as expected, the loop region shows much fluctuation (Figure 4). In WT as well as mutant, a increase in flexibility was observed in loops: (i) loop3 L3, connects H2 and H3, contains most of the active conserved residues and plays a major role in deacetylation process; (ii) loop4 (L4), connects H3 and helix 4 (H4) which present in the helical domain, undergoes a considerable changes to accommodate either the substrate or inhibitor; (iii) loop12 (L12) and loop14 (L14) present in the zinc-binding domain which connect B4 with β-sheet 5 (B5) and helix 9 (H9) with β-sheet 6 (B6), respectively; (iv) L15 linked B6 and helix 10 (H10), one of the conserved loop which connect the small and large domains, and loop 17 (L17) connect β-sheet 8 (B8) and β-sheet 9 (B9) placed in large domain. Among these flexible loops, L3 act as a front wall of C-site in the NAD^+ binding site and L15 plays an vital role in sirtuin function. The peak present in RMSF plot explains that the loop region is more flexible, however, it leaves the unchanged secondary structures but affects the nearby regions which is discussed in detail in conformational changes of the protein.

Structural features of functional domains in SIRT2

The protein deviation and fluctuation pattern in the nine systems are of a similar manner, hence it was difficult to find the significant difference in the behavior of proteins. Thus, changes in the key regions were analyzed from MD trajectories to examine an insight into the secondary structural behavior of protein.

Secondary structure comparative analysis between WT_Apo and WT_Sub

The secondary structure analysis was performed by using a do_dssp program from the GROMACS package based on the "Dictionary of Secondary Structure for Proteins." The residue G84-A91 (Helix2, H2) in Apo-form was changed into loop when presence of substrate (Figure 5(a)). From the above changes, we can predict that the space present in the active site of Apo-form was not enough, hence it changed and made suitable binding sites to accommodate NAD^+ for deacetylation process. Due to the substrate binding, H3 (G102-K109) and H8 (L172-A176) present in the linking region between small and large domains were slightly shifted and changed its secondary structure into loop (Figure 5(a)), respectively. The B3 in the large domain of Apo-form was varied to loop in presence of substrate, due to this the large groove volume was reduced and become compatible to accommodate NAD^+ for its cleavage and exchange process. B6 in Zn domain was changed into loop (Figure 5(a)), because of this structural change the H10 (A241-F251) was extended and connected one of the anti-parallel β-sheet (B6) in this domain with another β-sheet (B7) in Rossmann fold. Most of the helixes present are changed into loops, which indicate that the active site pocket was amplified in order to make suitable for NAD^+ binding.

Secondary structure comparative analysis of WT_Apo and WT_Inhi

In WT_Apo, H2 with the help of L3 connects B1 and H3 in large domain and helical domain, respectively.

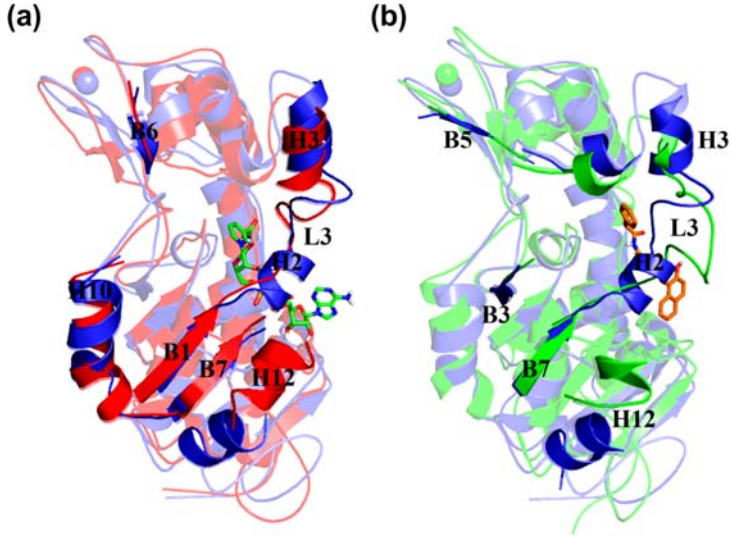

Figure 5. (a) Structural comparison of SIRT2 WT_Apo (blue) and WT_Sub (red), NAD^+: green stick. (b) WT_Inhi (green) and inhibitor: brown stick.

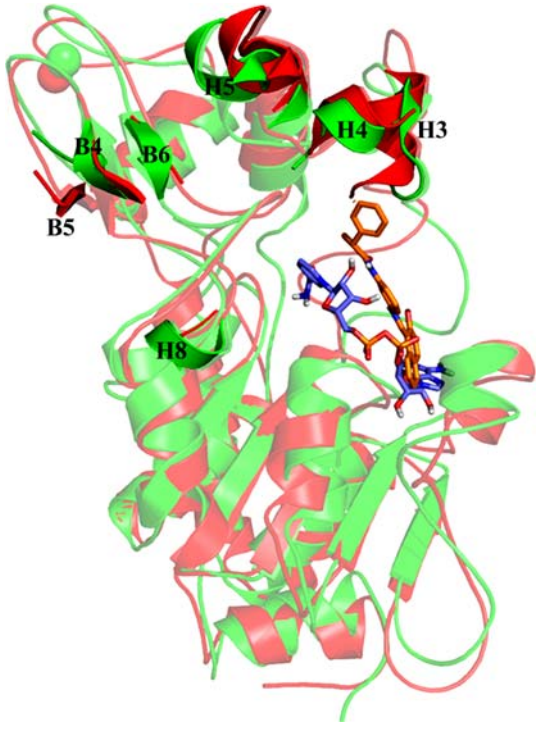

Figure 6. Comparison of wild type SIRT2 in complex with substrate (red) and inhibitor (green).

While inhibitor binds, the H2 is fully changed into loop and H3 was partially converted into loop that makes the F96 which is present in L3 to move outside of the active site and reduced its loop flexibility (Figure 5(b)). Due to the inhibitor binding, one of the anti-parallel β-sheet (B5) in zinc-binding domain was changed into loop because of this structural change the B3 and H10 in the large domain were converted into loop and extended its helical conformation, respectively (Figure 5(b)). We also observed that the H12 (Apo-form) present in large domain was partially changed into loop and shifted its position towards the helical domain due to the presence of inhibitor during MD simulation.

Secondary structure comparative analysis of WT_Sub and WT_Inhi

Numerous secondary structural changes are observed in presence of substrate and inhibitor. When analyzing the large domain, B3 present in WT_Apo was changed into loop in the presence of substrate and inhibitor (Figure 5 (a) and (b)). The H8 (L172-A176) linked small and large domains in WT_Apo remains same in the presence of inhibitor but changed into loop by substrate binding (Figure 6). In the small zinc-binding domain, out of three anti-parallel β-sheets, B6 was changed into loop and there is no structural changes observed in other two β-sheets in the presence of substrate (Figure 6). Instead of B6, B5 was changed into loop in the presence of inhibitor but B6 and B4 does not show any secondary structural changes. In case of helical domain, the H3 was

```
3GLR TPSGIPDFRSPGSGLYSNLQQYDLPYPEAIFELPFFFHNPKPFFTLAKELYP--GNYKPN
3GLS TPSGIPDFRSPGSGLYSNLQQYDLPYPEAIFELPFFFHNPKPFFTLAKELYP--GNYKPN
3GLT TPSGIPDFRSPGSGLYSNLQQYDLPYPEAIFELPFFFHNPKPFFTLAKELYP--GNYKPN
3GLU TPSGIPDFRSPGSGLYSNLQQYDLPYPEAIFELPFFFHNPKPFFTLAKELYP--GNYKPN
1J8F TSAGIPDFRSPSTGLYDNLEKYHLPYPEAIFEISYFKKHPEPFFALAKELYP--GQFKPT
1SZC TSCGIPDFRSPGTGLYHNLARLKLPYPEAVFDVDFFQSDPLPFYTLAKELYP--GNFRPS
1SZD TSCGIPDFRSPGTGLYHNLARLKLPYPEAVFDVDFFQSDPLPFYTLAKELYP--GNFRPS
2HJH TSLGIPDFRS-SEGFYSKIKHLGLDDPQDVFNYNIFMHDPSVFYNIANMVLP--PEKIYS
2H4H TPSGIPDFRGPNGIYKK--------YSQNVFDIDFFYSHPEEFYRFAKEGIFPMLQAKPN
2H59 TPSGIPDFRGPNGIYKK--------YSQNVFDIDFFYSHPEEFYRFAKEGIFPMLQAKPN
2H4J TPSGIPDFRGPNGIYKK--------YSQNVFDIDFFYSHPEEFYRFAKEGIFPMLQAKPN
2H4F TPSGIPDFRGPNGIYKK--------YSQNVFDIDFFYSHPEEFYRFAKEGIFPMLQAKPN
2H2I TPSGIPDFRGPNGIYKK--------YSQNVFDIDFFYSHPEEFYRFAKEGIFPMLQAKPN
2H2H TPSGIPDFRGPNGIYKK--------YSQNVFDIDFFYSHPEEFYRFAKEGIFPMLQAKPN
2H2G TPSGIPDFRGPNGIYKK--------YSQNVFDIDFFYSHPEEFYRFAKEGIFPMLQAKPN
2H2F TPSGIPDFRGPNGIYKK--------YSQNVFDIDFFYSHPEEFYRFAKEGIFPMLQAKPN
2H2D TPSGIPDFRGPNGIYKK--------YSQNVFDIDFFYSHPEEFYRFAKEGIFPMLQAKPN
1YC5 TPSGIPDFRGPNGIYKK--------YSQNVFDIDFFYSHPEEFYRFAKEGIFPMLQAKPN
1S7G AESGIPTFRGEDGLWRKYD-------PEEVASISGFKRNPRAFWEFSMEMKDKLFA-EPN
1YC2 AESGIPTFRGEDGLWRKYD-------PEEVASISGFKRNPRAFWEFSMEMKDKLFA-EPN
2B4Y AESGVPTFRGAGGYWRKWQ-------AQDLATPLAFAHNPSRVWEFYHYRREVMGSKEPN
2NYR AESGVPTFRGAGGYWRKWQ-------AQDLATPLAFAHNPSRVWEFYHYRREVMGSKEPN
     :  *:* **. .              .: :     *  .*  .: :             .
```

Figure 7. Multiple sequence alignment of sirtuin family. Human: 3GLR, 3GLS, 3GLT, 3GLU, 2NYR, 2B4Y, and 1J8F. Yeast: 2HJH, 1SZC, and 1SZD. *Archaeoglobus fulgidus*: 1YC2 and 1S7G. *Thermatoga maritima*: 2H2F, 2H2H, 2H2I, 2H2G, 2H2D, 2H4F, 2H4H, 2H4J, 2H59, and 1YC5. The black dot indicated the conserved F96 (numbering based on 1J8F).

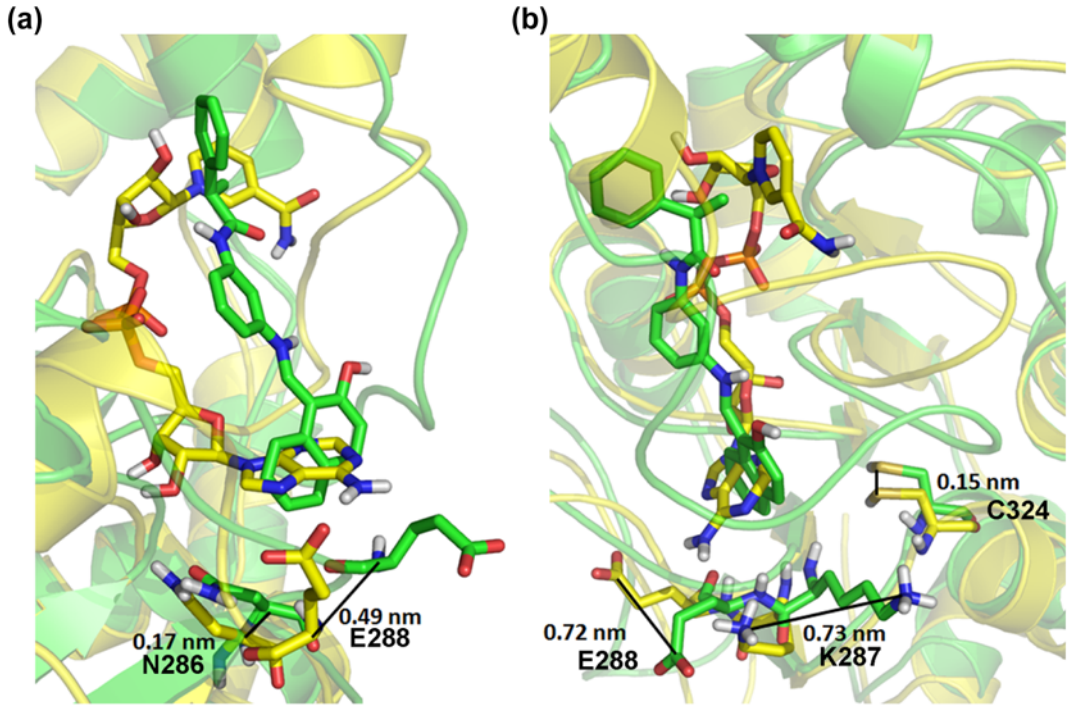

Figure 8. The deviation of A-site residues in the presence of NAD^+ and inhibitor in WT. (a) Cα distance of N286 and E288 in the presence of substrate (yellow) and inhibitor (green). (b) Side-chain distance of K287, E288, and C324 due to substrate (yellow) and inhibitor binding (green). NAD^+ and inhibitor are represented as stick.

partially distorted into loop which impacts a small deviation in helix 4 (H4) and helix 5 (H5). While inhibitor binds the critical amino acids (F96) was moved (nearly 20 Å) from its original position which might be the reason for H3 partial distortion. This H3 did not show any secondary structure changes in the presence of substrate.

From the structural analysis, it was confirmed that the small and large domains undergo a significant change in the secondary structures in the presence of substrate and inhibitor. Flexibility of the loop regions correlates well with other sirtuin families (Finnin et al., 2001) and the loops which are connecting the small and large domains have shown considerable changes. Hence, more care was given for the loop regions which may play a very pivotal role in the SIRT2 mechanism.

Analysis of NAD^+ binding mode in WT

In all systems, substrate helps the stability of SIRT2 throughout MD simulation which was highly evident from RMSD plots. NAD^+ interacts with most of the critical residues present in A-, B-, and C-sites of NAD^+ binding pocket and there is a strong π–π stacking effect between the phenyl rings of NAD^+ and F96. The adenosine moiety of NAD^+ had shown good interactions with A85, G86, R97, N286, K287, E288, E323, and C324 present in A-site. The residues Q167 and H187 present in B-site helps the nicotinamide region to enter into C-site by making interactions with phosphate groups of NAD^+, and the C-site residues are S87, F96, H149, N168, D169, and I170 interacts with nicotinamide part of NAD^+ to release the product.

The distance between phenyl ring of F96 and NAD^+ in initial structure was 0.61 nm, whereas after the first 3 ns of MD simulation the phenyl ring of F96 moves close to NAD^+ (distance 0.43 nm) and makes a strong aromatic (π–π) interaction. This expresses that F96 forms a tight stacking with NAD^+ which is one of the critical interactions in SIRT2 mechanism and play a vital role in the formation of C-site pocket. Due to the π–π interaction, the substrate complex was stabilized well and reduced the motion of F96 throughout MD simulation. In case of inhibitor, initially a 0.84 nm distance was found between phenyl group of F96 and inhibitor, after 3 ns the distance was increased to 1.30 nm. This distance constrains confirm that there is no chance for forming π-interaction between the phenyl ring of F96 and inhibitor. This indicates that F96 moves outside of the active site and this movement was supported by partial distortion of H3. Due to the movement of F96, the inhibitor complex, the formation of NAD^+ binding C-site collapsed.

Comparison of structural displacement in NAD^+ binding site with WT_Sub and WT_Inhi

NAD^+ binding pocket was conserved among all the sirtuin family which was confirmed by the multiple

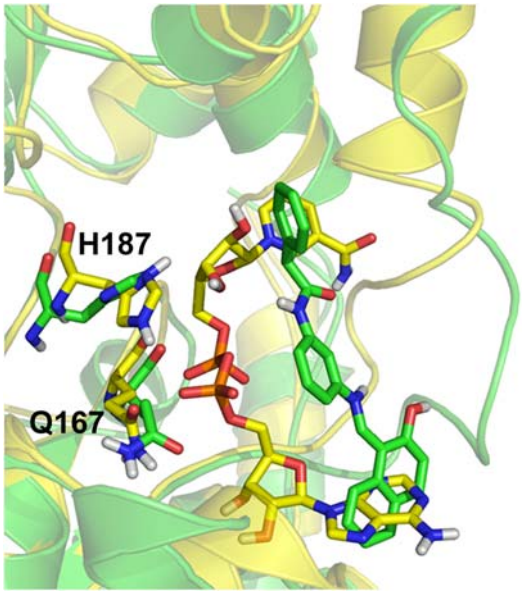

Figure 9. The deviation of B-site residues in the presence of WT_Sub (yellow) and WT_Inhi (green). NAD^+ and inhibitor are represented as stick.

sequence alignment of various sirtuin families (Figure 7). The NAD^+ binding pocket was commonly subdivided into three sites based on the interaction of adenine (A-site), ribose (B-site), and nicotinamide (C-site) the part of NAD^+ cofactor.

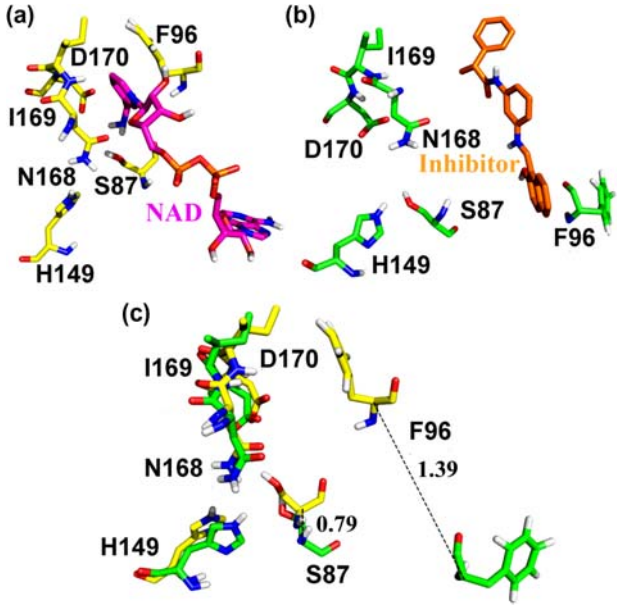

Figure 10. The deviation of C-site residues in WT (a) presence of substrate (yellow), NAD^+ (magenta), (b) presence of inhibitor (green), Inhibitor (brown), and (c) the deviation of the critical amino acids are represented as stick.

A-site

The A-site, suitable for adenine ring of NAD^+ binding, comprises of several important residues such as A85, G86, N286, K287, E288, E323, and C324. Among these, N286 and E288 amino acids forms hydrogen bond interactions with adenine ribose 2′ and 3′ hydroxyl group of NAD^+. Due to inhibitor binding, N286 and E288 were shifted to 0.17 and 0.49 nm which were confirmed by the Cα distance, respectively (Figure 8(a)). The ND2 of N286 in WT_Sub was deviated to 0.19 nm in WT_Inhi. The adenine based residues are G86 (0.12 nm), C324 (0.12 nm), K287 (0.28 nm), and E323 (0.12 nm) showed the considerable displacement while inhibitor binds, which confirmed by computing the distance between Cα atom. The side chain of C324, K287, and E288 have shown the deviation of 0.15, 0.73, and 0.72 nm, respectively (Figure 8(b)). The other two most interesting residues, R97 and A85, are poised to interact with phosphate O_2 of NAD^+ and moved to a distance (Cα) of 0.68 nm and 0.23 nm. Particularly, the side chain of R97 showed a significant displacement of 0.35 nm deviated from its original position when inhibitor binds.

B-site

It comprises of two critical residues such as H187 and Q167 makes a hydrogen bond with 3′ hydroxyl group of nicotinamide ribose and plays a key role in sirtuin mechanism. Mutation of these residues reduced SIRT2 deacetylation activity (Finnin et al., 2001) and also it helps the nicotinamide part of NAD^+ to occupy the C-site for deacetylation process. The Cα distance of H187 and Q167 in the presence of NAD^+ and inhibitor had shown a shift of 0.19 and 0.10 nm, respectively. The side chain of H187 was tilted by an angle of 4° due to inhibitor binding (Figure 9).

C-site

This site was focused on by many scientists and researchers to find the critical mechanism of sirtuin as well as to inhibit the sirtuin activity. From bacteria to humans the C-site of NAD^+ binding domain is exceedingly conserved in the sirtuin family. It does not have any contact with NAD^+, but is involved in the polarization and hydrolysis of the NAD^+ glycosidic bond (Finnin et al., 2001) with the help of highly conserved residues such as S87, P94, D95, F96, N168, and I169. Among these, N168, I169, and D170 form the rigid wall of the C-site and other residues like S87, P94, D95, and F96 present in loop (L3) region forms the front wall of C-site. The L3 shows a good conforma-

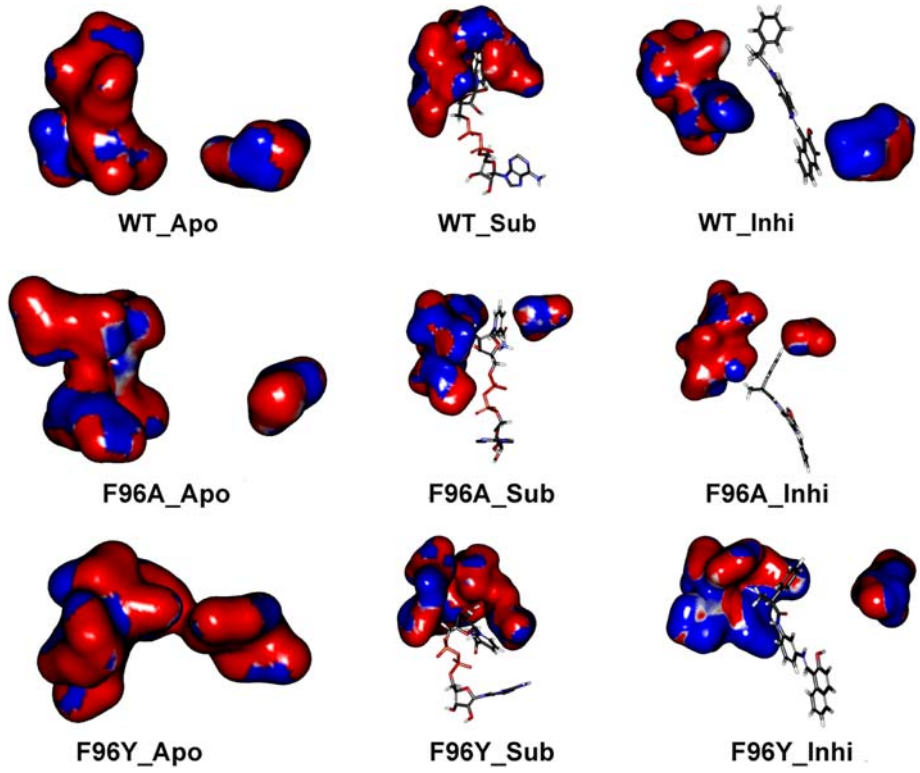

Figure 11. Electrostatic potential map indicates the assembly and disassembly of C pocket in the presence of NAD^+ and inhibitor. (a) Apo-form, (b) SIRT2–substrate, and (c) SIRT2–inhibitor.

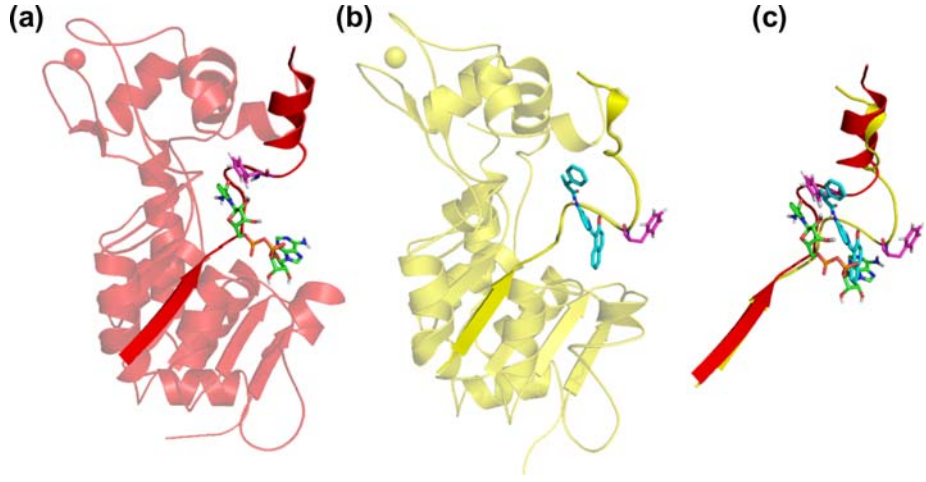

Figure 12. Structure represent of flexibility of L3. (a) SIRT2 in the presence of substrate indicates that the F96 in L3 come close to NAD^+, (b) SIRT2 in the presence of inhibitor indicates that the F96 in L3 move far away from its original position, and (c) overlay of SIRT2 in complex with substrate and inhibitor. NAD^+: green stick, inhibitor: cyan stick, and F96: magenta stick.

tional change in the presence of NAD^+ and inhibitor. Residues which are present in the rigid wall of the C-site have not shown much deviation due to inhibitor binding, the Cα distance was 0.07, 0.15, and 0.16 nm for N168, I169, and D170, respectively. But the residues placed in L3 loop showed an excellent movement in the presence of inhibitor which was confirmed by measuring the Cα distance for a residues S87 (0.79 nm), P94 (0.87 nm), D95 (0.98 nm), and F96 (1.39 nm) (Figure 10). The C-site might play a central

regulatory role in SIRT2 activity which proposes a structural basis for the action of small molecules that can either inhibit or stimulate the activity. The similar result was proposed by Avolos et al. (2005) in yeast sirtuin mechanism suggested that the human sirtuin also behave similarly like yeast.

Electrostatic potential map analysis

In order to elucidate the role of C-site, which plays an important role in the sirtuin mechanism electrostatic potential map was computed. It was assumed that the tight binding is achieved when the shape and chare distribution of the receptor cavity is optimally matched by the shape and charge distribution of the ligand molecule. Electrostatic potential surfaces are valuable in computer-aided drug design because they help in optimization of the electrostatic interactions between the protein and the ligand. Thus, SIRT2 APBS electrostatic potential was calculated (Baker et al., 2001) in the presence of substrates and inhibitor. DS calculates the electrostatic potential and maps the surface by color, where different colors are used to identify the different potentials. The most negative potential is colored red and the most positive is colored blue. The red color clearly indicated the strong negative charge which means the most electron-rich region of the molecule. The blue color represents the positive region which has the most electron-poor region of NAD^+. This indicates that the C-site pocket was relatively electron rich and the NAD^+ shows the relatively electron poor, which revealed that the negative charge of C-site can steadily hold tightly the positive charge of nicotinamide in NAD^+ (Figure 11). The electrostatic potential of SIRT2 was retained in the presence of inhibitor, but the inhibitor is not having a good positive charge, hence the assembly of C-site was distorted by moving the F96 residue (2.07 nm) from its original position and made the C-site not suitable for NAD^+ binding by disassembly its shape (Figure 12).

Critical role of L3 loop

One of the highly focusing loops in sirtuin family is L3 contains residues from G92 to T101 (G92-I93-P94-D95-F96-R97-S98-P99-S100-T101) which connects the helical domain with the large domain. It undergoes a significant structural change to facilitate the NAD^+ reactions of nicotinamide cleavage. The Cα distance for each residue in L3 region in the presence of NAD^+ and inhibitor are G92-0.61 nm, I93-0.79 nm, P94-0.87 nm, D95-

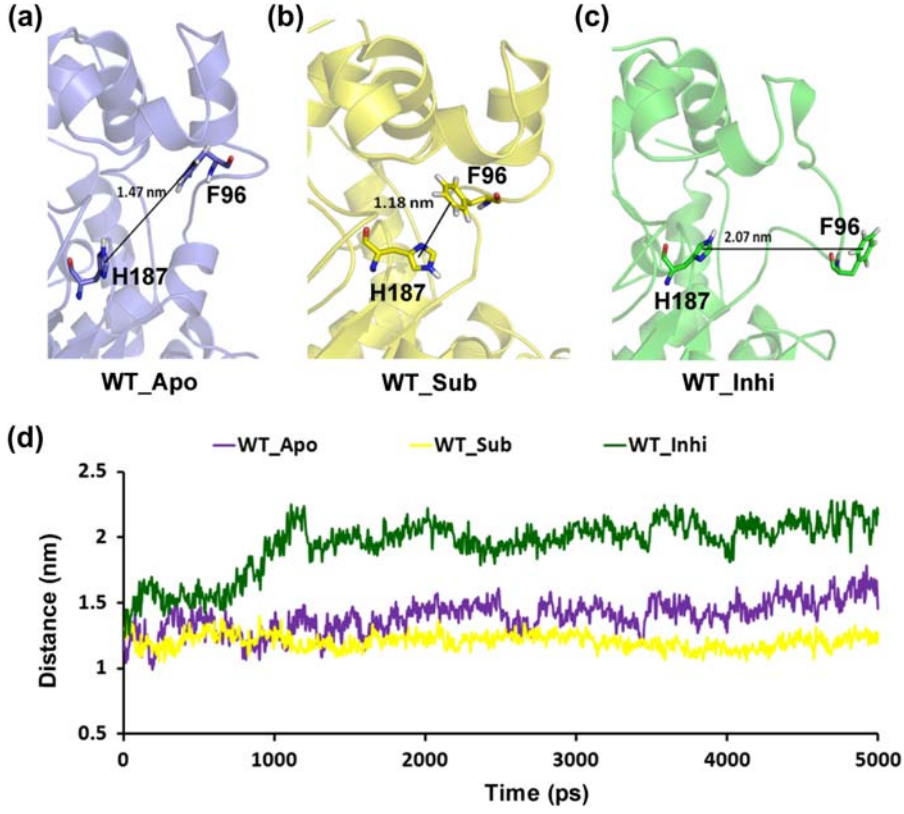

Figure 13. The distance between the F96 and H187 was clearly shown. (a) WT_Apo, (b) WT_Sub, (c) WT_Inhi, and (d) time trace of Cα–Cα distance between F96 and H187 in WT was plotted as a function of time to highlight the difference in orientation of the conserved F96 in the L3.

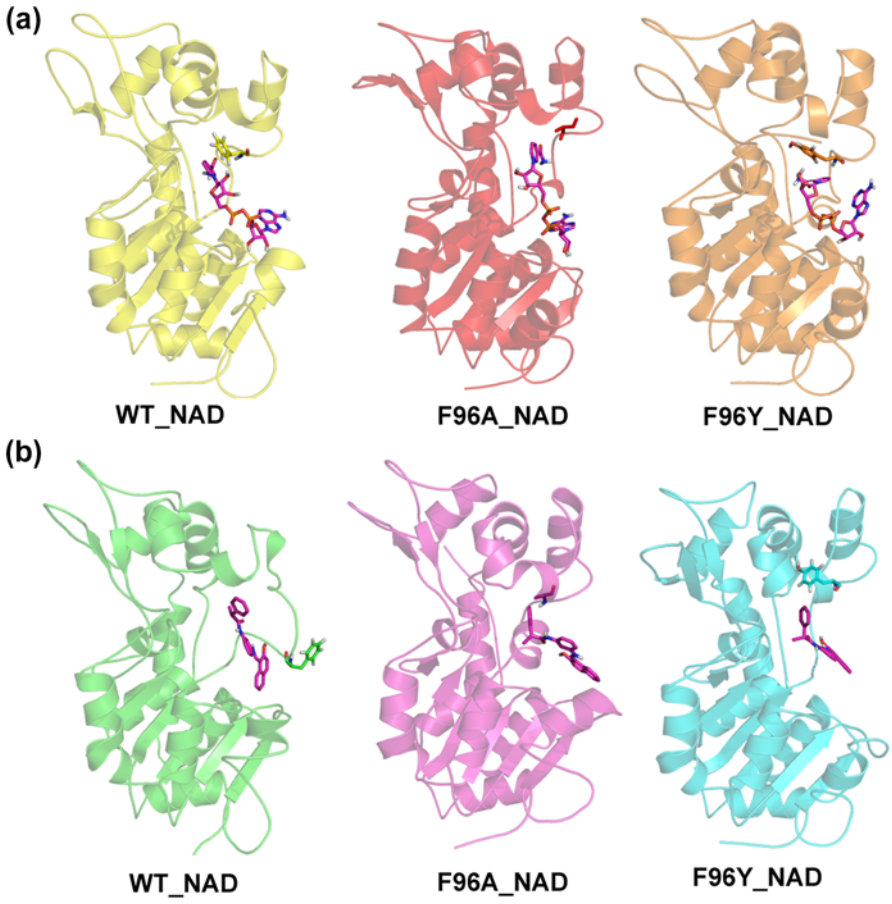

Figure 14. (a) π–π interactions between the phenyl ring of NAD^+ and F96, magenta: NAD^+. (b) π–π interaction was vanished due the distance between the phenyl ring of inhibitor and F96, magenta: inhibitor.

0.98 nm, F96-1.20 nm, R97-0.68 nm, P99-0.44 nm, S100-0.53 nm, and T101-0.38 nm. The binding of NAD^+ and inhibitor changes the flexibility of L3 and triggers the assembly and disassembly of C-site which was clearly explored by electrostatic potential map (Figure 11). Hence, we confirmed that the conformational flexibility of L3 plays a key role in the deacetylation process of SIRT2. The L3 becomes more labile which shows a significant shift to facilitate the NAD^+ reactions of nicotinamide cleavage and ADP-ribose transfer to acetate. The π–π interaction of nicotinamide part of NAD^+ and F96 entrapped the nicotinamide by flipping or the intermediated shift to the contracted conformation. Due to inhibitor binding, the π–π interactions were lost by moving F96 from its original position which makes the NAD^+ to bind in the nonproductive conformation.

Motion of F96 residue

F96, present in the front wall of C-site plays an important role in SIRT2 mechanism. To prove the conserved and importance of F96, multiple sequence alignment was performed using ClustalW for 22 sirtuin (Figure 7). Avalos et al. (2005) have experimentally proved the importance of F96 in enzymatic activity of sirtuin mechanism by stabilizing and orienting the nucleophile attack in NAD^+. In our study, a substantial shift of F96 has been observed when compared Cα distance of F96 in the presence of substrate and inhibitor which makes us takes special attention. H187 and F96 present in the third and first crossover loops which connects the small Zn-binding domain and helical domain with large domain, respectively, and acts as a potential barrier for the nicotinamide exchange reaction. In WT_Apo, the average distance between F96 and H187 is 1.47 nm does not move far away from its starting point and maintained an average distance of 1–1.50 nm over the entire simulation. In the case of WT_Sub, F96 moves close to H187 in order to make an assembly of the C-site and the average distance between F96 and H187 was 1.18 nm suggests that L3 and L12 narrowing the groove between the large and small domains which might be suitable for the deacetylation process (Figure 13). Conversely, in WT_Inhi, F96

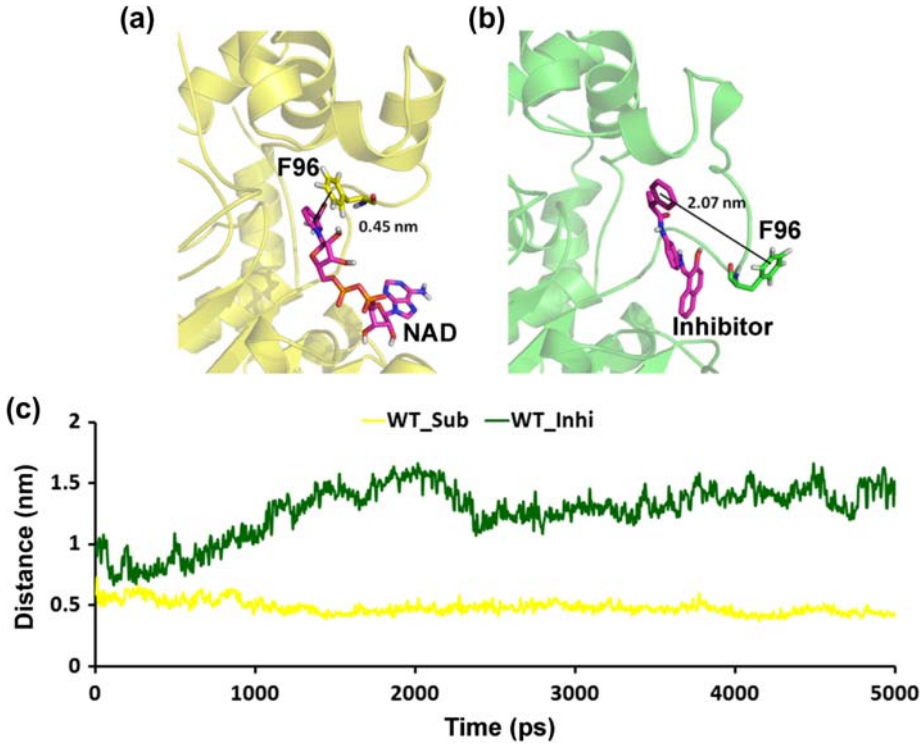

Figure 15. The distance between the phenyl ring of F96 and NAD^+/inhibitor in WT was plotted as a function of time. (a) WT_Sub, (b) WT_Inhi, and (c) 2D plot comparison between WT_Sub and WT_Inhi.

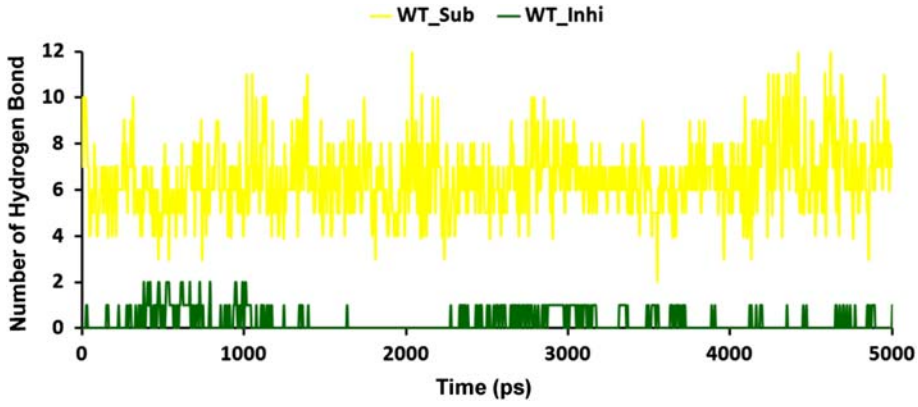

Figure 16. The total number of intermolecular hydrogen bond interactions exhibited by NAD^+ and inhibitor in complex with SIRT2 (WT) as a function of time.

exhibits high mobility with an average distance of 2.07 nm between F96 and H187. This increase of distance due to inhibitor binding might be a chance for disassembly of C-site which was confirmed by comparing it with WT_Sub. Hence, we concluded that the binding of inhibitor widening the space between small and large domains as well as it moves the F96 in the front wall of the C-site (L3) which is not suitable for deacetylation process. Another interesting role of F96 is the formation of π–π interaction with nicotinamide part of NAD^+ (Figure 14(a)), which helps the nicotinamide to occupy a suitable place for the cleavage of glycosidic bond in sirtuin deacetylation process. In addition, distance between the phenyl group of F96 and nicotinamide ring of NAD^+ was 0.42 nm, but the distance between phenyl group F96 and inhibitor was increased to 1.50 nm (Figure 15(a) and (b)). The graph in Figure 15(c) clearly indicates that the distance between the phenyl group of F96 and NAD^+ was maintained throughout the simulation within the average distance of 0.45 nm. In the case of WT_Inhi, initially the distance between phenyl group of F96 and

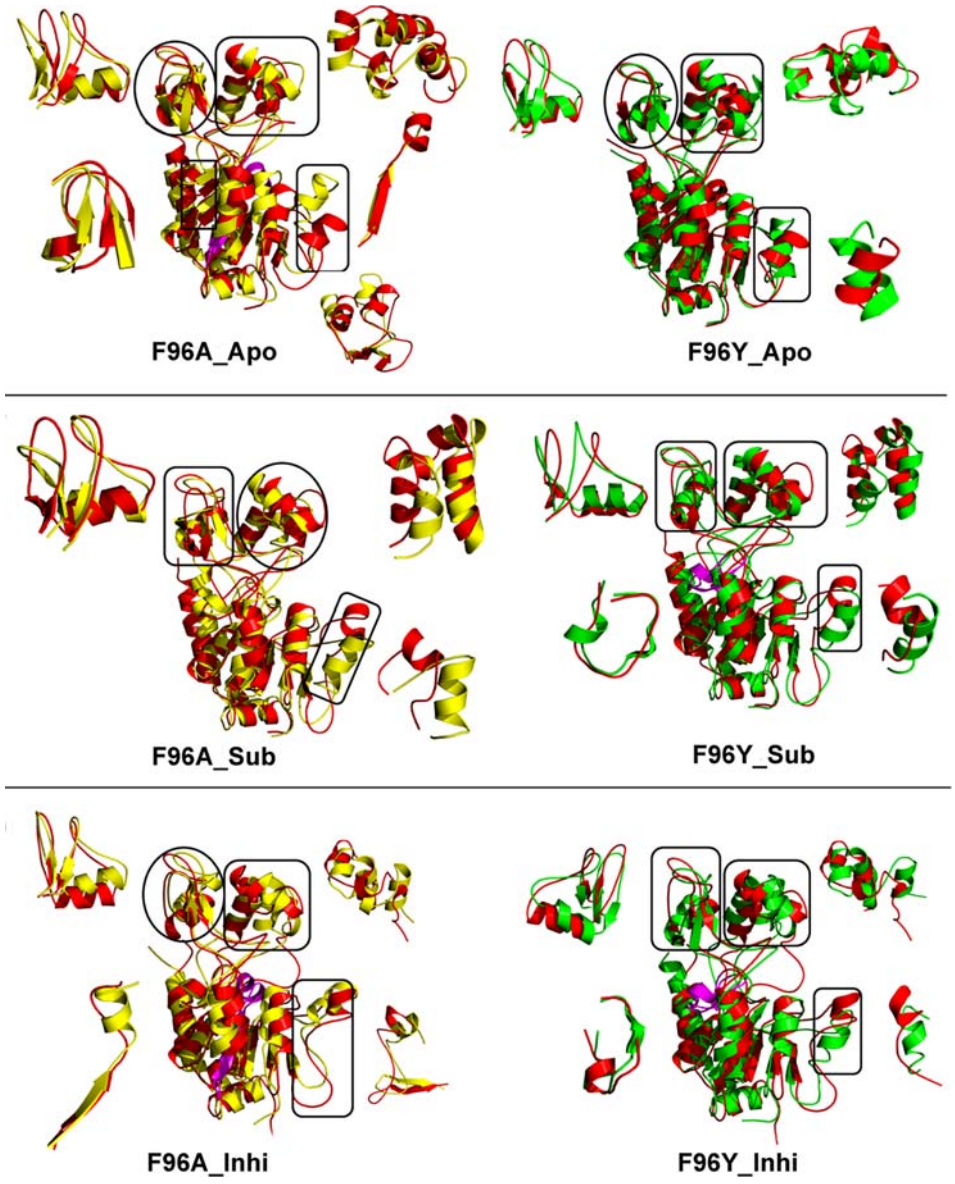

Figure 17. Comparison of cartoon representation of the structure and domain changes due to mutation of F96. WT, red; F96A, yellow; and F96Y, green.

inhibitor was 1 nm, after 1 ns it shows a greater difference and maintained throughout the simulation. This result also supports that inhibitor binding moves F96, as a result the good π–π interaction was abolished. From the overall analysis, it was clearly indicated that F96 is responsible for the assembly and disassembly of C-site. The conformation and the mobility of F96 are important for deacetylation process and this residue might play a central role in SIRT2 mechanism.

Hydrogen bond analysis

Hydrogen bond analyses reveal the binding affinity of protein ligand is one of the structural properties of target protein that is essential for specificity with a ligand. Since, hydrogen bonds are directly responsible for specificity and affinity between protein and substrate/ligands. In order to characterize the interactions between NAD^+–SIRT2 and inhibitor–SIRT2, we calculated the time dependent patterns of hydrogen bonding during simulation. The geometric criterion for the formation of H-bonds is common with an H-acceptor distance less than 0.30 nm and donor–H-acceptor angle larger than 120° (Yeung et al., 2004). In WT_Sub, the number of hydrogen bond was maintained (nearly 10–12) but in the case of WT_Inhi, initially the number of hydrogen bond was 2, but after 1 ns only one hydrogen bond was maintained throughout the simulation (Figure 16).

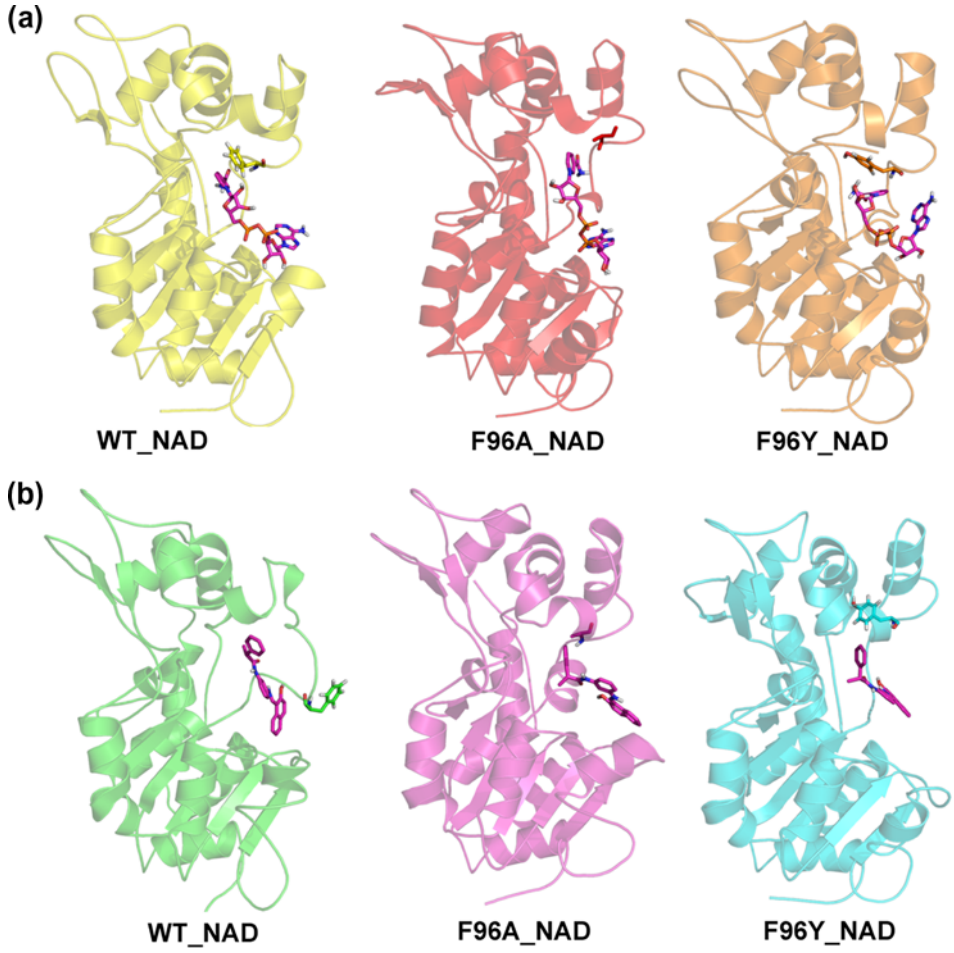

Figure 18. (a) π–π Interactions between the phenyl ring of NAD^+ and F96, magenta: NAD^+. (b) π–π Interaction was vanished due to the distance between the phenyl ring of inhibitor and F96, magenta: inhibitor.

Mutational analysis

In order to affirm the importance of F96 in SIRT2 catalytic mechanism it was mutated to alanine (F96A) and tyrosine (F96Y). Cartoon representation of Figure 17 showed the structural changes in Apo-form and complex structures due to mutations compared with WT. Focusing on NAD^+ binding site, three residues in A-site have shown a considerable deviation when compared with the both mutations such as the distance between R97 and the phosphate O_2 group was 0.97 nm but in case of F96A_Sub and F96Y_Sub was 1.30 nm and 0.94 nm, respectively. The distance between adenine ribose 2′, 3′ OH and N286, E288 showed a value of 0.41 nm and 0.81 nm in WT_Sub, but the distance between the N286 and adenine ribose 2′ OH was increased in F96A (0.57 nm) and decreased in F96Y_Sub (0.30 nm). In case of E288, both mutations (F96A-0.42 nm and F96Y-0.41 nm) have shown a distance less than WT_Sub. In B-site, Q167 and H187 form hydrogen bonds with 3′OH nicotinamide ribose which helps the NAD^+ to place a nicotinamide in a suitable position. The distance between the Q167, H187, and 3′OH nicotinamide ribose in WT_Sub was 0.59 nm, F96A_Sub (0.56 nm), and F96Y_Sub (0.60 nm). From the above results, it was suggested that the A- and B-sites are not showing much difference due to F96 mutations.

Interestingly, the F96 has shown a good divergence which was confirmed by calculating the distance between residue 96 and NAD^+ and phenyl group of inhibitor. In F96Y, the distance between Y96 and NAD^+ was 0.44 nm which was suitable for the formation of π–π interaction. In case of F96A_Sub, the distance was 0.74 nm between the NAD^+ and A96 which clearly indicates that the alanine mutation fails to produce π–π interaction important for the flipping of nicotinamide in cleavage process (Figure 18(a)).

In addition, by computing the distance between residue 96 and H187 present at the neck of C-site. In the presence of substrate, WT shows a distance of 1.18 nm, F96A and F96Y have shown a distance of 1.37 and

1.13 nm, respectively. Comparing the WT with F96A and F96Y distinctly shows that the difference in alanine mutation was not able to form a suitable binding pocket for NAD^+, as well as in case of F96Y the distance between two residues was smaller than WT; this may be due to the hydroxyl group of tyrosine residue.

In case of inhibitor, the distance between residue 96 and H187 was so close in F96A (1.19 nm) and 1.66 nm for F96Y, but in WT_Inhi it was 2.08 nm (Figure 18(b)). In addition, the electrostatic analysis of C-site NAD^+ binding pocket clearly revealed that F96A was not able to form the assembly of C-site whereas in F96Y, the hydroxyl group of tyrosine was placed inside the cavity that made the C-site shrink which is not suitable for the cleavage of nicotinamide from NAD^+ (Figure 11). The movement of residue 96 due to inhibitor binding was very similar in case of tyrosine mutation, when we compared the Cα-distance of residue 96 and C23 of inhibitor in F96A and F96Y shows a distance of 0.83 and 1.08 nm, respectively. From this analysis, one can see that A96 comes close to inhibitor than in substrate, but in case of F96Y behaves similarly to WT. The above analysis suggests that any aromatic or bulky amino acids were not able to form an assembly of C-site pocket for cleavage of nicotinamide from NAD^+. From overall analysis, we concluded that the F96 is important for SIRT2 mechanism; mutation of this residue with any other amino acids with the similar properties could decrease or abolish the SIRT2 activity.

Hence, we believe that the above structural insight of SIRT2 complex will be very helpful to design a novel and potent inhibitor to inhibit SIRT2 activity. We have arrived at a number of general guidelines that should help to direct the selection of the novel and potent inhibitors for SIRT2. Following are the important criteria for small molecules to become potent inhibitors

(1) The molecules which move the F96 present in L3 which was present in the front wall of C-site from its original position.
(2) Molecules which disturbed the assembly of C-site.
(3) Molecules which increases the distance between the H187 and F96.
(4) Overall any small molecules which distorted the assembly of C-site will be a potent inhibitor for SIRT2.

Conclusions

Sirtuin is a promising drug target in the treatment of cancer, Alzheimer's, and also in several age related diseases. The last decade has witnessed tremendous progress in understanding the biological functions of sirtuin and its mechanism. X-ray crystallography structure provided only the structural insights into their unique properties, but fails to explain the dynamics behavior of SIRT2. Hence, MD simulations were performed to provide a structural basis for the activation and inhibition of SIRT2 in the presence of substrate and inhibitor. In this study, GROMACS MD simulation package with GROMOS96 force field and explicit water molecules were used. The comparative study of SIRT2 in WT and mutants revealed the conformational changes in SIRT2. The large, small zinc binding and helical domains undergo various conformational changes in the presence of substrate and inhibitor. Due to NAD^+ binding, large groove between the large and small domains was narrowed which makes a suitable place for NAD^+ deacetylation reaction. While inhibitor binding the groove was widened, as a result, the assembly of C-pocket was distorted. NAD^+ and inhibitor bring F96 present in the L3 loop close and far away from H187 make the assembly and disassembly of C-pocket, respectively. Due to this process, the nicotinamide deacetylation reaction was activated and inhibited. Focusing on all the structural changes and displacement (WT, F96A, and F96Y) we concluded that the F96 plays a vital role in binding mechanism of SIRT2. The information of the L3 pliability at atomic level obtained in this study could provide valuable clues to design potent and selective inhibitors for SIRT2.

The computational techniques help in drug design process to dramatically widen the chemical space and reduce the number of candidates for experimental validation. Combining the pharmacophore modeling, virtual screening, and molecular docking techniques are one of inexpensive, fast alternative reputable methods in drug discovery to enhance the efficiency in lead identification and optimization for various targets. Structure details of protein will be important in the drug design process, our result revealed the clear view of the binding orientation and interaction site of NAD^+/inhibitor. The interaction site was characterized by several critical interactions like hydrogen bond interactions and lipophilic side chains complement reflects the hydrophobic nature of NAD^+ binding pocket and inhibitors in the active site of SIRT2. These structural details will be helpful to design a novel and potent SIRT2 inhibitors using various computational techniques mentioned above. Mainly this structural insight will be useful in structure-based pharmacophore modeling and is one of the productive tool to discover the compounds with improved potency and pharmacokinetic properties.

Acknowledgments

This research was supported by Basic Science Research Program (2009-0073267), Pioneer Research Center Program

(2009-0081539), and Management of Climate change Program (2010-0029084) through the National Research Foundation of Korea (NRF) funded by the Ministry of Education, Science and Technology (MEST) of Republic of Korea. And this work also supported by the Next-Generation BioGreen21 Program (PJ008038) from Rural Development Administration (RDA) of Republic of Korea.

References

Avalos, J.L., Bever, K.M., & Wolberger, C. (2005). Mechanism of Sirtuin inhibition by Nicotinamide: Altering the NAD+ Cosubstrate specificity of a Sir2 Enzyme. *Molecular Cell, 17*, 855–868.

Avalos, J.L., Boeke, J.D., & Wolberger, C. (2004). Structural basis for the mechanism and regulation of Sir2 enzymes. *Molecular Cell, 13*, 639–648.

Avalos, J.L., Celic, I., Muhammad, S., Cosgrove, M.S., Boeke, J.D., & Wolberger, C. (2002). Structure of a Sir2 enzyme bound to an acetylated p53 peptide. *Molecular Cell, 10*, 523–535.

Baker, N.A., Sept, D., Joseph, S., Holst, M.J., & McCammon, J.A. (2001). Electrostatics of nanosystems: Application to microtubules and the ribosome. *Proceedings of the National Academy of Sciences of the United States of America, 98*, 10037–10041.

Berendsen, H.J.C., Postma, J.P.M., van Gunsteren, W.F., DiNola, A., & Haak, J.R. (1984). Molecular dynamics with coupling to an external bath. *The Journal of Chemical Physics, 81*, 3684–3690.

Berendsen, H.J.C., Postma, J.P.M., van Gunsteren, W.F., & Hermans, J. (1981). Interaction models for water in relation to protein hydration. *Intermolecular Forces, 11*, 331–342.

Berendsen, H.J.C., van der Spoel, D., & van Drunen, R. (1995). GROMACS: A message-passing parallel molecular dynamics implementaion. *Computer Physics Communications, 91*, 43–56.

Berman, H.M., Westbrook, J., Feng, Z., Gilliland, G., Bhat, T. N., Weissig, H., … Bourne, P.E. (2000). The protein data bank. *Nucleic Acids Research, 28*, 235–242.

Brooks, B., Bruccoleri, R., Olafson, B., States, D., Swaminathan, S., & Karplus, M. (1983). CHARMM: A program for marcromolecular energy, minimization, and dynamics calcualtions. *Journal of Computational Chemistry, 4*, 187–217.

Brunet, A., Sweeney, L.B., Sturgill, J.F., Chua, K.F., Greer, P. L., Lin, Y., … Greenberg, M.E. (2004). Stress-dependent regulation of FOXO transcription Factors by the SIRT1 deacetylase. *Science Aging Knowledge Environment, 303*, 2011–2015.

Dryden, S.C., Fau-Nahhas, S.C., Nahhas, F.A., Goustin, A.S., & Tainsky, M.A. (2003). Role for Human SIRT2 NAD-dependent deactylase activity in control of mitotic exit in the cell cycle. *Molecular and Cellular Biology, 23*, 3173–3185.

Finnin, M.S., Donigian, J.R., & Pavletich, N.P. (2001). Structure of the histone deacetylase SIRT2. *Nature Structural & Molecular Biology, 8*, 621–625.

GROMACS 3.1.4. (2002). Department of biophysical chemistry. University of Groninger, Nijenborgh 4, 9747 AG Groningen, The Netherlands. Retrieved from http://www.gromacs.org

Grozinger, C.M., Chao, E.D., Blackwell, H.E., Moazed, D., & Schreiber, S.L. (2001). Identification of a class of small molecule inhibitors of the sirtuin family of NAD-dependent deacetylases by phenotypic screening. *Journal of Biological Chemistry, 276*, 38837–38843.

Guarente, L. (2007). Sirtuins in aging and diseases. *Cold Spring Harbor Symposia on Quantitative Biology, 72*, 483–488.

Haigis, M.C., & Guarente, L.P. (2006). Mammalian sirtuins - emerging roles in physiology, aging, and calorie restriction. *Genes and Development, 20*, 2913–2921.

Hess, B., Bekker, H., Berendsen, H.J.C., & Fraaije, J.G.E.M. (1997). LINCS: A linear constraint solver for molecular simulations. *Journal of Computational Chemistry, 18*, 1463–1472.

Hiratsuka, M., Inoue, T., Toda, T., Kimura, N., Shirayoshi, Y., Kamitani, H., … Oshimura, M. (2003). Proteomics-based idnetification of differentially expressed genes in human gliomas: Down-regulation of SIRT2 gene. *Biochemical and Biophysical Research Communications, 309*, 558–566.

Huhtiniemi, T., Suuronen, T., Rinne, V.M., Wittekindt, C., Lahtela-Kakkonen, M., Jarho, E., … Leppanen, J. (2008). Oxadiazole-carbonylaminothioureas as SIRT1 and SIRT2 inhibitors. *Journal of Medicinal Chemistry, 51*, 4377–4380.

Huhtiniemi, T., Wittekindt, C., Laitinen, T., Leppänen, J., Salminen, A., Poso, A., & Lahtela-Kakkonen, M. (2006). Comparative and pharmacophore model for deacetylase SIRT1. *Journal of Computer-Aided Molecular Design, 20*, 589–599.

Imai, S., Armstrong, C.M., Kaeberlein, M., & Guarente, L. (2000). Transcriptional silencing and longevity protein Sir2 is an NAD-dependent histone deacetylase. *Nature, 403*, 686–689.

Landry, J., Sutton, A., Tafrov, S.T., Heller, R.C., Stebbins, J., Pillus, L., & Sternglanz, R. (2000). The silencing protein SIR2 and its homologys are NAD-dependent protein deacetylases. *Proceedings of the National Academy of Sciences of the United States of America, 97*, 5807–5811.

Lindahl, E., Hess, B., & van der Spoel, D. (2001). GROMACS 3.0: A package for molecular simulation and trajectory analysis. *Journal of Molecular Modeling, 7*, 306–317.

Longo, V.D., & Kennedy, B.K. (2006). Sirtuins in aging and age-related disease. *Cell, 126*, 257–268.

Mai, A., Massa, S., Lavu, S., Pezzi, R., Simeoni, S., Ragno, R., … Sinclair, D.A. (2005). Design, synthesis, and biological evaluation of sirtinol analogues as class III histone/protein deacetylase (sirtuin) inhibitors. *Journal of Medicinal Chemistry, 48*, 7789–7795.

McGovern, B.K., Fau-Shoichet, S.L., & Shoichet, B.K. (2003). Information decay in molecular docking screens against holo, apo, and modeled conformations of enzymes. *Journal of Medicinal Chemistry, 46*, 2895–2907.

Metoyer, C.F., & Pruitt, K. (2008). The role of sirtuin proteins in obesity. *Pathophysiology, 15*, 103–108.

Michishita, E., Park, J.Y., Burneskis, J.M., Barrett, J.C., & Horikawa, I. (2005). Evolutionarily conserved and nonconserved cellular localizations and functions of human SIRT proteins. *Molecular Biology of the Cell, 16*, 4623–4635.

Miyamoto, S., & Kollman, P. (1992). Settle: An analytical version of the SHAKE and RATTLE algorithm for rigid water models. *Journal of Computational Chemistry, 13*, 952–962.

Motta, M.C., Divecha, N., Lemieux, M., Kamel, C., Chen, D., Gu, W., … Guarente, L. (2004). Mammalian SIRT1 represses forkhead transcription factors. *Cell, 116*, 551–563.

Outeiro, T.F., Kontopoulos, E., Altmann, S.M., Strathearn, K. E., Amore, A.M., … Kazantsev, A.G. (2007). Sirtuin 2 inhibitors rescue alpha-synuclein-mediated toxicity in models of Parkinson's disease. *Science, 317*, 516–519.

Rodgers, J.T., Lerin, C., Haas, W., Gygi, S.P., Spiegelman, B. M., & Puigserver, P. (2005). Nutrient control of glucose homeostasis through a complex of PGC-1α and SIRT1. *Nature, 434*, 113–118.

Sakkiah, S., Thangapandian, S., John, S., & Lee, K.W. (2011). Identification of critical chemical features for aurora kinase-B inhibitors using hip-hop, virtual screening and molecular docking. *Journal of Molecular Structure, 985*, 14–26.

Sakkiah, S., Baek, A., & Lee, K.W. (2012). Pharmacophore modeling and molecular dynamics simulation to identify the critical chemical features against human sirtuin2 inhibitors. *Journal of Molecular Structure, 1011*, 66–75.

Sakkiah, S., Krishnamoorthy, N., Gajendrarao, P., Thangapandian, S., Lee, Y., Kim, S., … Lee, K.W. (2009). Pharmacophore mapping and virtual screening for SIRT1 activators. *Bulletin of the Korean Chemical Society, 30*, 1152–1156.

Satoh, A., Brace, C.S., Ben-Josef, G., West, T., Wozniak, D.F., Holtzman, D.M., & … (2010). SIRT1 promotes the central adaptive rsponse to diet restriction through activation of the dorsomedial and lateral nuclei of the hypothalamus. *The Journal of Neuroscience, 30*, 10220–10232.

Schuttelkopf, A.W., & Aalten, D.M.F.v. (2004). PRODRG: A tool for high-throughput crystallography of protein-ligand complexes. *Acta Crystallographica. Section D, Biological Crystallography, 60*, 1355–1363.

Smellie, A., Teig, S.L., & Towbin, P. (1995). Poling: Promoting conformational variation. *Journal of Computational Chemistry, 16*, 171–187.

Van Der Spoel, D., Lindahl, E., Hess, B., Groenhof, G., Mark, A.E., & Berendsen, H.J.C. (2005). GROMACS: Fast, flexible, and free. *Journal of Computational Chemistry, 26*, 1701–1718.

Vaquero, A., Scher, M.B., Lee, D.H., Sutton, A., Cheng, H.L., Alt, F.W., … Reinberg, D. (2006). SirT2 is a histone deacetylase with preference for histone H4 Lys 16 during mitosis. *Genes & Development, 20*, 1256–1261.

Vaziri, H., Dessain, S.K., Ng Eaton, E., Imai, S.I., Frye, R.A., Pandita, T.K., … Weinberg, R.A. (2001). hSIR2(SIRT1) functions as an NAD-dependent p53 deacetylase. *Cell, 107*, 149–159.

Venkatachalam, C.M., Jiang, X., Oldfield, T., Waldan, M., & LigandFit, N. (2003). LigandFit: A novel method for the shape-directed rapid docking of ligands to protein active sites. *Journal of Molecular Graphics and Modelling, 21*, 289–307.

Westphal, C.H., Dipp, M.A., & Guarente, L. (2007). A therapeutic role for sirtuins in diseases of aging? *Trends in Biochemical Sciences, 32*, 555–560.

Witt, O., Deubzer, H.E., Milde, T., & Oehme, I. (2009). HDAC family: What are the cancer relevant targets? *Cancer Letters, 277*, 8–21.

Yeung, F., Hoberg, J.E., Ramsey, C.S., Keller, M.D., Jones, D. R., Frye, R.A., & Mayo, M.W. (2004). Modulation of NF-κB-dependent transcription and cell survival by the SIRT1 deacetylase. *EMBO Journal, 23*, 2369–2380.

Zhao, K., Harshaw, R., Chai, X., & Marmorstein, R. (2004). Structural basis for nicotinamide cleavage and ADP-ribose transfer by NAD(+)-dependent Sir2 histone/protein deacetyalses. *PNAS, 101*, 8563–8568.